Published in final edited form as:
J Control Release. 2012 August 20; 162(1): 208–217. doi:10.1016/j.jconrel.2012.06.020.

Effects of block copolymer properties on nanocarrier protection from *in vivo* clearance

Suzanne M. D'Addio[a], **Walid Saad**[a], **Steven M. Ansell**[b], **John J. Squiers**[a], **Douglas Adamson**[a], **Margarita Herrera-Alonso**[a], **Adam R. Wohl**[c], **Thomas R. Hoye**[c], **Christopher W. Macosko**[d], **Lawrence D. Mayer**[b], **Christine Vauthier**[e], and **Robert K. Prud'homme**[a,*]

[a]Chemical and Biological Engineering, Princeton University, Princeton, NJ 08544 USA

[b]Celator Pharmaceuticals Corporation, 1779 W 75[th]Ave., Vancouver, B.C., V6P6P2, Canada

[c]Department of Chemistry, University of Minnesota, Minneapolis, MN 55455 USA

[d]Department of Chemical Engineering, University of Minnesota, Minneapolis, MN 55455 USA

[e]University Paris Sud, Physicochimie, Pharmacotechnie, Biopharmacie, UMR 8612, Chatenay-Malabry, F-92296, France

Abstract

Drug nanocarrier clearance by the immune system must be minimized to achieve targeted delivery to pathological tissues. There is considerable interest in finding *in vitro* tests that can predict *in vivo* clearance outcomes. In this work, we produce nanocarriers with dense PEG layers resulting from block copolymer-directed assembly during rapid precipitation. Nanocarriers are formed using block copolymers with hydrophobic blocks of polystyrene (PS), poly-ε-caprolactone (PCL), poly-D,L-lactide (PLA), or poly-lactide-*co*-glycolide (PLGA), and hydrophilic blocks of polyethylene glycol (PEG) with molecular weights from 1.5 kg/mol to 9 kg/mol. Nanocarriers with paclitaxel prodrugs are evaluated *in vivo* in *Foxn*1^{nu} mice to determine relative rates of clearance. The amount of nanocarrier in circulation after 4 h varies from 10% to 85% of initial dose, depending on the block copolymer. *In vitro* complement activation assays are conducted in an effort to correlate the protection of the nanocarrier surface from complement binding and activation and *in vivo* circulation. Guidelines for optimizing block copolymer structure to maximize circulation of nanocarriers formed by rapid precipitation and directed assembly are proposed, relating to the relative size of the hydrophilic and hydrophobic block, the hydrophobicity of the anchoring block, the absolute size of the PEG block, and polymer crystallinity. The *in vitro* results distinguish between the poorly circulating PEG_{5k}-PCL_{9k} and the better circulating nanocarriers, but could not rank the better circulating nanocarriers in order of circulation time. Analysis of PEG surface packing on monodisperse 200 nm latex spheres indicates that the sizes of the hydrophobic PCL, PS, and PLA blocks are correlated with the PEG blob size, and possibly the clearance from circulation. Suggestions for next step *in vitro* measurements are made.

*Author for Correspondence, Department of Chemical Engineering, Princeton University, Princeton, NJ 08544 USA Tel: (609) 258-4577 Fax: (609) 258-0211 prudhomm@princeton.edu.

Supplemental Information Available

Further details on HPLC analysis, prodrug stability, nanocarrier toxicity, stoichiometric loading of nanocarriers, and log*P* calculations are available in Supplemental Information. This material is available free of charge *via* the Internet at http://www.sciencedirect.com.

Keywords

nanocarrier; polyethylene glycol; complement activation; *in vivo* circulation; nanoparticle; block copolymer; polycaprolactone; polylactic acid; stealth

1. Introduction

Nanocarrier formulations are attractive because they can be targeted to disease sites where localized drug release maximizes therapeutic effectiveness, and also minimizes off-site exposure of healthy tissue to potentially toxic therapeutic agents. The fate of nanocarriers is determined by a number of physiochemical properties, including particle size, surface charge, and core properties. Interactions with various serum proteins may result in clearance by resident macrophage action, hepatic filtration, extravasation, diffusion, kidney excretion, or by active transport across tight junctions (Fig. 1) [1]. Drug release is influenced by the physical properties of the drug and possible interactions with the delivery vehicle [2]. Accumulation, drug release, and clearance occur on various timescales, and ultimately determine the overall efficacy or toxicity of a formulation (Fig. 1). Accumulation of the nanocarrier at the target site is a prerequisite for optimal administration. In the case of passive targeting by the enhanced permeation and retention (EPR) effect [3, 4], circulation times longer than several hours are required to ensure a sufficient number of passes through the target site to enable accumulation. For active targeting, protection of the nanocarrier from non-specific opsonization is required to ensure that targeting is effected by only the ligand or antibody presented on the nanocarrier surface. One requirement to extend circulation times and permit accumulation is that nanocarriers escape non-specific opsonization.

Early in the characterization of nanocarriers, it was established that uncoated hydrophobic nanocarriers are rapidly cleared from circulation, largely by the mononuclear phagocyte system (MPS), and that a hydrophilic corona around the particle core extended circulation times [5]. One of the most popular corona components is polyethylene glycol (PEG) [6]. Obtaining well protected nanocarriers requires the formation of a dense brush of PEG to shield the underlying particle surface and delay molecular recognition [7]. Several PEG coating approaches have been reported. With liposomes, the PEG-lipid "stealth" components can only be incorporated to a maximum of ~10 mol% before the liposomal bilayer is disrupted [8]. In addition, PEG-lipids are known to partition off of the surface of liposomes [9, 10] and the protection from clearance is not complete. On solid nanocarriers, there are fundamental limitations to the density of PEG chains that can be grafted onto a nanocarrier surface since chain insertion through a brush layer is kinetically unfavorable [11]. PEG densities above the density of the "mushroom" regime [12] are generally not possible. High brush densities are attainable by processes that involve polymerizing off of a surface [13, 14], but these methods are difficult to combine with drug loading for therapeutic particles.

While a goal for the nanocarrier is long circulation *in vivo*, a major need in the area of optimized stealth protection with PEG is a method to predict the relative duration of *in vivo* circulation times for nanocarriers from *in vitro* assays. A promising *in vitro* assay is the complement activation assay, which measures the activation of complement upon binding to surfaces. While any number of serum components may adsorb to nanocarrier surfaces to activate clearance by the MPS, the complement system is thought to be a major mechanism of nanocarrier clearance [7]. The use of whole serum in the complement assay, with the spectrum of proteins present, may more accurately represent the complexity of *in vivo* testing than assays based on less complex media. Complement assays are widely used [15–

20], and the extent to which they can provide a link between *in vivo* and *in vitro* results is one focus of this study.

The second major focus of this study is to understand the relationship between block copolymer structure and clearance for nanocarriers protected by amphiphilic diblock copolymers. The nanocarrier system we are studying is made by the kinetically-controlled, block copolymer-directed assembly termed Flash NanoPrecipitation (FNP) [21, 22]. The FNP process is scalable and has been demonstrated for a wide variety of amphiphiles and drug compounds [2, 23–26]. The process is described in more detail below. While PEG protection on liposomes and other nanocarrier systems has been investigated, there have been no studies of PEG protection on nanocarriers made by kinetically-controlled, rapid precipitations using FNP. PEG layers established on FNP nanocarriers may provide greater protection against clearance than PEG layers on nanocarriers created by alternate assembly processes. Prior results have shown that the diffusion-limited aggregation of amphiphilic block copolymers during FNP results in a PEG density near the brush regime [27], which is higher than can be achieved by conventional slow assembly processes or grafting. The PEG assembly in FNP is driven by the adsorption of the hydrophobic block onto the nanocarrier surface. Therefore, we study the effects of hydrophobic block type and molecular weight (M*w*) and PEG M*w* on *in vitro* and *in vivo* performance. To eliminate size as a variable, nanocarriers of approximately equal sizes were prepared as shown in Fig. 2b. To decouple the effects of drug release and nanocarrier clearance, we use nanocarriers in this study with a hydrophobic paclitaxel prodrug core, which is known not to be released during circulation [2]. Tuning the release kinetics of paclitaxel prodrugs, the associated efficacy, and toxicity was the focus of a previously published study [2]. In this work, we focus on four hydrophobic block types; 1) polystyrene (PS), 2) poly-D,L-lactide (PLA), 3) poly-ε-caprolactone (PCL), and 4) poly-lactide-*co*-glycolide (PLGA) of various molecular weights, and we consider PEG molecular weights of 2k, 3k, and 5k.

2. Materials and Methods

2.1. Block copolymers

We use the nomenclature "PEG_m-XXX_n" to refer to block copolymers, where *m* is the M*w* of the PEG block in g/mol, XXX is the particular hydrophobic block type, and *n* is the M*w* of the hydrophobic block in g/mol. Polyethylene glycol-*b*-polystyrene (PEG_{5k}-$PS_{1.5k}$) was synthesized according to published procedure [28]. Polyethylene glycol-*b*-poly-D,L-lactide polymers (PEG_{5k}-PLA_{2k}, PEG_{5k}- PLA_{5k}, PEG_{5k}-PLA_{10k}) and polyethylene glycol-*b*-poly-lactide-*co*-glycolide (PEG_{5k}-$PLGA_{8k}$) were synthesized by a novel polymerization of a poly(ethylene glycol) (PEG) macroinitiator, using 1,8-diazabicyclo[5.4.0]-undec-7-ene (DBU) as catalyst with a controlled co-monomer feed for the PLGA block [29, 30]. The synthesis and characterization of PEG_{5k}-PLA_{20k} was previously reported [31]. Polyethylene glycol-*b*-ε-polycaprolactone (PEG_{2k}-PCL_{3k}, PEG_{5k}-PCL_{5k}, PEG_{5k}-PCL_{7k}, PEG_{5k}-PCL_{9k}) block copolymers were synthesized by ring-opening polymerization of ε-caprolactone, catalyzed by stannous octoate, using monomethoxy poly(ethylene glycol) as a macro initiator according to published procedure [32]. $PEG_{4.8k}$-$PS_{3.8k}$, PEG_{5k}-$PS_{9.5k}$, and PEG_{5k}-PCL_{3k} were obtained from Polymer Source (Montreal, Quebec) and PEG_{3k}-PS_{1k} was obtained from Goldschmidt (Essen, Germany).

2.2. Prodrug synthesis

The paclitaxel-vitamin E succinate prodrug (hereafter referred to as "the prodrug") was prepared by esterification of the terminal carboxyl group on vitamin E succinate (VES, Sigma Aldrich. St. Louis, MO) and the C-2′ hydroxyl group on paclitaxel in the presence of DMAP and DIPC (see Supplemental Information). The synthesis has been described

previously [2]. The reaction was carried out by dissolving VES (66.3 mg, 0.125 mmol) in methylene chloride (20 mL) at 0 °C, followed by the addition of diisopropylcarbodiimide (29 μL, 0.19 mmol). Finally, paclitaxel (146 mg, 0.17 mmol, Indena S.p.A. Milan, Italy) and dimethylaminopyridine (32 mg, 0.26 mmol) were added. The solution was allowed to reach room temperature and react for 16 h. The reaction mixture solution was washed with 0.1 N hydrochloric acid, dried with magnesium sulfate, and then dried in vacuo. ^{1}H NMR spectra were recorded in $CDCl_3$ on a Bruker Avance 400.

2.3. Prodrug nanocarrier formulation

Prodrug nanocarriers for *in vivo* experiments were prepared using the FNP scheme in a multi inlet vortex mixer, MIVM, (Fig. 2a) to precipitate prodrug (10 mg/mL), VES (10 mg/mL) and a diblock copolymer (20 mg/mL) from tetrahydrofuran (THF, HPLC Grade, Fisher Scientific. Pittsburgh, PA). The THF solution was fed *via* a digital syringe pump (Harvard PHD 2000) at 12 mL/min and mixed with three streams of water, each at 40 mL/min, in the MIVM (Fig. 2a). Prior to use, water was purified *via* 0.2 μm filtration and four stage deionization to a resistivity of 17.8 MΩ or greater (NANOpure Diamond, Barnstead International. Dubuque, IA). To remove THF from the mixture, 20 mL of the suspension was dialyzed in Spectra/Por® 6–8kD MWCO regenerated cellulose dialysis tubing (Spectrum Labs. Rancho Dominguez, CA) against 1L of continuously stirred water, which was refreshed 6 times over 24 h. Particle size measurements were obtained using a Nicomp 380 ZLS particle sizer (Vancouver, British Columbia). The average particle size is reported in Table 1 with one standard deviation of the log-normal distribution to indicate the distribution width. The suspensions were stored at 4 °C.

2.4. HPLC analysis to quantify prodrug concentrations

Plasma samples or prodrug nanocarrier suspensions of 50 μL were mixed with 150 μL of diluent (methanol:acetonitrile, 2:1 v/v) by vigorous vortexing followed by centrifugation at 10,000 x g for 10 min. Supernatant (20 μL) was analyzed using a Phenomenex SynergiFusion reverse phase analytical column monitored by UV detection at 227 nm. Chromatography was conducted with a 1 mL/min mobile phase of methanol and 10 μM sodium acetate buffer (pH 5.6), from an initial solvent ratio of 70:30 to a final ratio of 97:3 over 20 min. With this method, peaks corresponding to free paclitaxel, VES, and prodrug could be resolved and integrated, where the area under the curve was directly proportional to concentration. The area under the peak in the chromatograms was correlated for known concentrations of VES from 0.4 – 10 μg/mL and paclitaxel from 0.1 – 10 μg/mL (see Supplemental Information). The resolution of the peaks was independent of concentration and was not affected by the presence of the block copolymers (see Supplemental Information). The column temperature was set at 30 °C. Samples were kept in the autosampler compartment at 4 °C.

2.5. In vivo plasma assay

Fox*n*1^{nu} mice were obtained from Harlan (Indianapolis, IN). All animal experiments were conducted according to protocols approved by the University of British Columbia's Animal Care Committee and in accordance with the current guidelines established by the Canadian Council of Animal Care. Prior to injection, prodrug nanocarriers in DI water were 0.2 μm filtered to sterilize and the concentration was determined by HPLC (Table 1). Athymic nude mice (n = 3 per formulation) were administered a drug dose of 40 mg/kg at a volume of 200 μL/20 g *via* the lateral tail vein, which was warmed under a lamp for 1–2 min to increase blood flow. Mice were sacrificed 4 h following injection and 500–700 μL of blood was extracted and centrifuged at 2500 rpm for 15 min. Plasma was recovered and 50 μL aliquots were analyzed by HPLC for prodrug content. The initial prodrug concentration in plasma was 0.09 mg/mL with 10% variation due to filtration and transfer steps. Concentration

values for the conjugate at the time of injection (t = 0 h) was calculated based on 75 mL/kg of mouse blood volume, with a plasma content of 55% of blood, which is equivalent to 4.125% of body weight [2]. The results are reported in terms of % of initial dose. Three mice were used per time point, and the error bars associated with the results correspond to ± the standard deviation of the average.

2.6. Prodrug free nanocarrier preparation

Since nanocarrier protection is conferred by the PEG corona, and the hydrophobicity of the conjugated paclitaxel and vitamin E are similar, inert core nanocarriers were prepared for the complement activation studies. The compositions were tuned to produce nanocarriers that match the size of the active drug nanocarriers. Vitamin E was included at the particular concentrations in THF in order to adjust the final size, so that all nanocarriers had comparable sizes as shown in Table 2 and Fig. 2b. A THF solution containing the proper concentrations of block copolymer, $c_{BCP,THF}$, vitamin E (97%, Sigma. St. Louis, MO), $c_{VE,THF}$, and nile red (99%, Fisher Scientific. Pittsburg, PA), $c_{NR,THF}$, at 12 mL/min was mixed with three streams of water at 40 mL/min each in the MIVM (Fig. 2a). To remove THF from the mixture, 20 mL of the suspension was dialyzed in Spectra/Por® 6–8kD MWCO regenerated cellulose dialysis tubing (Spectrum Labs. Rancho Dominguez, CA) against 1L of continuously stirred water, which was refreshed 6 times over 24 h. Nanocarrier suspensions were concentrated using a Nanosep Omega 100k ultrafiltration membrane (Pall Corporation. Exton, PA) to remove 100–400 μL water *via* centrifugation at 5,000 × g for 15 min from a 500 μL aliquot (Fig. 2a). The retentate was resuspended to 500 μL with additional dilute nanocarrier suspension and the centrifugation process was repeated until the desired final concentration was achieved. Dynamic light scattering (DLS) was used to determine the intensity-weighted particle size distribution (PSD) (Fig. 2b) and average particle diameter for each nanocarrier suspension. A drop of each concentrated sample was diluted in 1 mL of water and the size was measured using a ZetaSizer Nano ZS (Malvern Instruments. Worcestershire, U.K.). The intensity-weighted average diameters were between 59 and 98 nm.

Nile red was included at 0.10 – 0.25 wt% of the nanocarrier formulation to facilitate quantification of nanocarrier concentrations during synthesis by measuring nile red fluorescence by excitation at 485 nm using a Hitachi F-7000 Fluorescence Spectrophotometer (Hitachi High-Technologies Corporation). The nile red was not used in subsequent *in vivo* nor *in vitro* complement assays. A 10 μL sample of the nanocarrier suspension was added to 10 mL of THF to dissolve the nanocarriers and solubilize the incorporated nile red. The measured intensity of emission was used to calculate the mass concentration of nile red, c_{NR}, in the original nanocarrier suspension, using a linear correlation. Since all nanocarrier components are incorporated stoichiometrically into the nanocarrier formulation during precipitation in FNP (see Supplemental Information), the measured c_{NR} allows us to calculate the total nanocarrier particle mass concentration in the original suspension, c_P, by

$$c_P/c_{NR} = \left(c_{BCP,THF} + c_{VE,THF} + c_{NR,THF}\right)/c_{NR,THF} \quad (1)$$

Nanocarrier formulations were concentrated to 11–19 mg/mL solids (Table 2) by removing water *via* centrifugation, as described above. The filtrates for each sample were pooled and the intensity of the fluorescence emission at 590 nm was measured without dilution. The amount of nanocarrier lost in the filtrate was found to be less than 1% of the mass in the concentrates.

The total volume of solids in the suspension (c_P/ρ), was calculated using the total mass concentration, c_P (from fluorescence measurements) and an approximate density, ρ, of 1 g/cm^3. The number concentration of nanocarriers in the suspension, N, was calculated by dividing the total volume of solids in the suspension (c_P/ρ) by the volume per particle ($4\pi r^3/3$), using the radius, r, obtained by DLS. The surface area in each suspension was then calculated as the product of the surface area per particle, S_P, and the number concentration of nanocarriers in the suspension, N,

$$S_P N = \left(4\pi r^2\right)(c_P/\rho)\left(4/3\,\pi r^3\right)^{-1} = 3\frac{c_P}{\rho r} \quad (2)$$

The calculated surface area per mL of solution is summarized for each formulation in Table 2.

2.7. Complement assay

Complement activation tests were performed at a nanocarrier surface area of 3,000 cm^2/mL with a volume of 100 μL and the complete experiment was performed 3 times for each nanocarrier formulation. Serum was prepared from human plasma obtained from the Etablissement Français du Sang (Kremlin Bicêtre) by adding 200 μL of calcium chloride (1 M) in Tris buffer (100 mM pH 7.4) to 10 mL of plasma.

Human serum (50 μL) and veronal buffer (diethylmalonylurea 5 mM, calcium chloride 0.15 mM, magnesium chloride 0.5 mM, sodium chloride 150 mM, pH 7.4) (50 μL) were added to the diluted sample of nanocarriers and incubated for 60 min at 37 °C under gentle agitation. After incubation, 5 μL of the sample was analyzed by 2D immunoelectrophoresis to measure complement activation. The first-dimension electrophoresis was performed on an agarose gel slab (7 × 13 cm) at 1% prepared in tricine buffer (Tricine 27 mM, Tris 63 mM, Calcium lactate 1 mM, pH 8.6). For the second dimension, the band of migration was cut from the gel slab and placed on a Gelbond® film (7 × 5 cm, GE Healthcare). A solution containing 1% agarose gel (Sigma Life Science) in tricine buffer and anti-human C3 polyclonal antibody from goat (Sigma Aldrich) was added on the remaining free area of the gel bond film. After hardening, the gel slab was submitted to the second-dimension electrophoresis. Electrophoresis was performed using tricine buffer as the running buffer in an electrophoresis apparatus Pharmacia LKP Multiphor II. For the first dimension, the electric field (600 V, 16 mA) was applied for approximately 1 h using a Pharmacia electrophoresis power supply (EPS600). The migration was stopped when bromophenol blue used as marker had migrated over 6 cm. For the second dimension, the electric field (500 V, 16 mA) was applied for 18 h. After electrophoresis, the gel slab was dried with filter paper and stained by a coomassie blue staining method.

The gel slab was scanned three times at high resolution and the numerical images were then analyzed to evaluate the area of each peak appearing on the electrophoregram using the Image J software [33]. A ratio, R, was calculated from the analysis of each gel slab, in which A_{C3ab} corresponds to the area under the activated fragment peak (Fig. 3a, right peak) and A_{C3} is the area under the native protein peak (Fig. 3a, left peak),

$$R_{PEG_m-XXX_n} = A_{C3ab} / (A_{C3} + A_{C3ab}) \quad (3)$$

The R ratio obtained for each nanocarrier was used to calculate the Complement Activation Factor (CAF), on a scale from 0 to 100, taking into account the ratios R determined for a

negative control sample ($R_- = 0.08 \pm 0.01$) and for a positive control sample ($R_+ = 0.98 \pm 0.02$),

$$CAF_{PEG_m-XXX_n} = 100 \times \left(R_{PEG_m-XXX_n} - R_-\right) / (R_+ - R_-) \quad (4)$$

2.8. Calculation of logP values

The log*P* values for the hydrophobic components were calculated using Molinspiration Cheminformatics property calculations, which have been validated and widely used [34]. The program enables the calculation of the log*P* values for polymers as a function of M*w*. The details of implementing the calculation are given in the Supplemental Information. The M*w* dependence of log*P*, as well as other polymer properties such as the glass transition temperature, *Tg*, occur because of the difference between the end groups and the central chain segments. Therefore, the log*P* of a very large M*w* polymer asymptotes toward a value for an infinite M*w* chain.

2.9. Coating latex spheres and Baleux Assay for analysis of PEG density on nanocarriers

The Baleux assay, which creates a PEG:iodine complex, is used to quantify the PEG surface density on the nanocarrier surfaces, which is achieved as the block copolymer adsorbs on the hydrophobic core of the nanocarriers. To calibrate sample absorbance with polymer concentration, PEG-PCL, PEG-PLA, and PEG-PS micelles were prepared by mixing 3 streams of water at 36 mL/min with 1 solution of polymer in THF (5.3 mg/mL) at 12 mL/min in the MIVM. The micelles were subsequently diluted 1:10 with 10 vol% THF in water and then 1:2 with DI water, for a final composition of 3.3 % THF in water. This THF concentration was found to be low enough to affect neither the Baleux assay nor the micellization of free polymer in solution [27]. To 1 mL dilutions of micelles in 3% THF in water, 25 μL of the Baleux assay reagent (0.25 g I_2 + 0.5 g KI in 25 mL of 3.3% THF-water) was added [35]. The calibration samples were allowed to sit for precisely 5 min before measuring sample absorbance at λ = 500 nm.

The MIVM was used to deposit block copolymer PEG layers on monodisperse hydrophobic latex spheres. The monodisperse sphere is used as a "core," since greater precision can be achieved in determining the total surface area in the dispersion with the monodisperse latex than in the somewhat polydisperse precipitated core of the actual FNP organic core nanocarrier [27]. Deposition is achieved by mixing two streams of DI water and one stream with 0.111 wt% aqueous suspension of surfactant-free latex spheres (200 nm, Invitrogen™. Eugene, OR) at 36 mL/min with a fourth stream of THF at 12 mL/min which contained 5.3 mg/mL PEG_{5k}-PCL_n, PEG_{5k}-PLA_n, or PEG_{5k}-PS_n. After coating the latex, the sample was diluted as described for the calibration samples to obtain a suspension in 3.3% THF. To measure the amount of polymer on the latex, 1 mL of suspension was centrifuged for 30 min at 20,000 × g (Centrifuge 5430R, Eppendorf) to settle the coated latex. A 0.9 mL portion of the supernatant was gently removed, and the pellet was resuspended in 0.9 mL of 3.3% THF-water. The resuspended pellet sample retained 0.1 mL (10%) of supernatant. The concentration of PEG in the supernatant and the resuspended pellet was measured by adding 25 μL of the Baleux assay reagent and then measuring absorbance at λ = 500 nm after precisely 5 min. The amount of PEG in the pellet was adjusted by subtracting the PEG remaining in the 0.1 mL of the supernatant, which was measured separately. The Baleux assay was run on three replicate samples of the supernatant and pellet for each formulation. Each day, 25 μL of Baleux assay was added to 1 mL of 3.3% THF-water to establish the baseline absorbance of the assay, which was subtracted from each subsequent measurement

during that day, to account for fluctuations in baseline Baleux absorbance. Concentrated solutions were diluted to maintain the assay absorbance reading between $0.1 < AU < 1$.

The polymer chain aggregation number per latex particle was found by dividing the measured mass of PEG by the PEG M*w* and the known number of latex particles. The resulting aggregation numbers, *n*, were then used to calculate the blob size of the polymer at the interface, ξ_i, which is the diameter of a free polymer coil assuming no interactions between neighboring chains. The polymer blob size is determined by equating the area covered by the polymer to the area available for polymer coverage [27],

$$n\pi(\xi_i/2)^2=4\pi(D_{latex}/2+\xi_i/2)^2 \quad (5)$$

where D_{latex} is the diameter of the uncoated latex sphere.

3. Results and Discussion

Decoupling the drug release from the nanocarrier and the nanocarrier clearance in circulation is a promising strategy to tuning nanocarrier efficacy. The subjects of rate of release, efficacy, and associated toxicity were investigated in an earlier study by Ansell *et al.*, where it was found that the prodrug release was determined by the physical and chemical properties of the prodrug, given the same stabilizer used during FNP to stabilize the particles [2]. The rate of prodrug partitioning out of the nanocarrier was directly correlated to *in vivo* antitumor efficacy, and the most efficacious formulation had a higher effective maximum tolerated dose of paclitaxel, relative to the conventional Cremophor paclitaxel formulation [2]. In this current study, we hold the nanocarrier core size constant and vary the stabilizer formulation in order to investigate the clearance of the delivery vehicle, rather than the release kinetics of the drug

3.1. In vivo nanocarrier circulation

Previously, the paclitaxel-VES prodrug nanocarriers were labeled with the nonexchangeable lipophilic label tritiated cholesteryl hexadecylether [36], and it was found that the paclitaxel-VES prodrug and nanocarrier were both cleared from circulation at the same rate over 24 h [2]. Therefore, the prodrug remains associated with the nanocarrier and the quantified prodrug at 4 h in circulation corresponds to the presence of the nanocarriers. The hydrolysis kinetics for the prodrug were also investigated, and it was found that the prodrug was well protected in the nanocarrier core, resulting in negligible hydrolysis at pH 7.4 at 37 °C (see Supplemental Information). The nanocarriers also protected the prodrug from significant cleavage by esterases, with only 10% cleavage of the prodrug over 50 h in serum at 37 °C (see Supplemental Information). The clearance kinetics (i.e. concentration vs. time over 24 h) of these FNP paclitaxel prodrugs for a single block copolymer has been reported previously [2], with the most stable formulation circulating with a 24 h half life. The time point at 4 h was chosen to permit screening of a variety of samples and directly determine if the criteria for formulations with $t_{1/2} > 4$ h had been met.

The quantified amount of prodrug remaining in circulation after 4 h is shown in Fig. 4. Nanocarrier circulation varies significantly with block copolymer chemistry and M*w*. Given equivalent 5k PEG blocks, circulation varies from 9.7% to 58%, depending on the hydrophobic PCL block size. Conversely, for the same 3k PCL hydrophobic block, a 5k PEG block almost triples the amount in circulation relative to the 2k PEG (58% vs. 19%). The longest circulating nanocarriers are stabilized by the PEG_{3k}-PS_{1k}; 85% of the nanocarriers are still in circulation after 4 h. Clearly, neither the stabilizing PEG M*w* nor the hydrophobic block M*w* alone are sufficient criteria to explain the observed circulation

results. These results, and the *in vitro* complement results to be shown below, suggest four effects that control circulation and "stealth" behavior of nanocarriers made by FNP: 1) the relative anchoring area of the hydrophobic block to that of the solvated PEG chain, 2) the hydrophobicity or anchoring strength of the hydrophobic block relative to the solvation energy of the hydrophilic block, 3) the absolute M*w* of the PEG block, and 4) the amorphous/crystalline nature of the hydrophobic block.

(1) *The relative anchoring area of the hydrophobic block to that of the solvated PEG chain.* As mentioned previously, the PCL block copolymers, which all have 5k PEG chains, show an inverse dependence of circulation on M*w* of the hydrophobic block. It might have been expected that increasing the M*w* of the hydrophobic block would provide better protection and reduce opsonization due to the decreased solubility of the block copolymer in the aqueous phase, which might decrease its propensity to partition off of the nanocarrier surface. Yet we find that decreasing block size increases protection. An explanation is found by considering the surface area occupied at the hydrophobic interface by the hydrophobic block. From our previous studies [26, 37], calculations based on solubility parameters would indicate that the hydrophobic chains are miscible with the nanocarrier core, so that the hydrophobic tail would occupy an area approximately equal to the square of its radius of gyration. The smaller area of the lower M*w* hydrophobic block results in a more laterally compressed, dense PEG layer [38]. The density of PEG in the brush layer as a function of PCL M*w* for these polymers after coating a latex sphere by FNP was quantified and supports this hypothesis. This dense layer efficiently prevents opsonin adsorption. However, decreasing the hydrophobic block M*w* to too low a value would result in inadequate anchoring energy and deprotection of the nanocarrier surface. This is observed in the partitioning of the less hydrophobic Pluronic® block copolymers off of nanocarrier surfaces due to inadequate anchoring energy [26].

(2) *The hydrophobicity or anchoring strength of the hydrophobic block relative to the solvation energy of the hydrophilic block.* The anchoring strength of the hydrophobic block is governed by the enthalpic contribution to the Gibbs free energy, which is determined by the M*w* of the block and its hydrophobicity (see Supplemental Information for a discussion of enthalpic and entropic contributions that show the enthalpic contribution is the dominant factor in determining the hydrophobic block anchoring). The combined factors of M*w* and hydrophobicity can be captured by calculating the partition coefficient, *P*, of the block between octanol and water which is reported as log*P*. A log*P* for each block type as a function of M*w* was calculated using the Molinspiration program [34] (see SI for details of modeling). In Fig. 5, the calculated log*P* values for hydrophobic anchoring blocks as a function of M*w* are plotted. Even at M*w* = 1.5k, the log*P* of the polystyrene block is greater than 11; it is the most hydrophobic of the blocks. PCL is an order of magnitude less hydrophobic than PS at the same M*w*. To obtain the same hydrophobicity as a 3k PS block, a 9k PCL is required, and higher than 10k for PLA. A PLGA 50/50 block has a very low log*P* of 2.6 for a 5k PLGA block. This is consistent with the use of PLGA as a controlled release matrix, where erosion by relatively rapid hydrolysis is desired [39]. We have also calculated the log*P* of the polypropylene oxide (PPO) block of the commonly used Pluronic® and added it to Fig. 5. The range of the PPO block M*w* available in Pluronic® is 0.9k – 3.6k [40] and these blocks are also relatively weakly hydrophobic. This is the reason that Pluronic® with large PEG blocks can partition off of nanocarrier surfaces, have relatively low critical micelle concentration values, and allow relatively rapid clearance. In contrast, for FNP we employ large enough hydrophobic blocks that they are frozen on the nanocarrier surface once kinetically anchored. The data in Fig. 5 show that obtaining equal hydrophobicity for PLA and PS requires such a large PLA block that the PEG chain occupies too small an area on the hydrophobic surface to prevent opsinon adsorption. Merely increasing PEG length to compensate for the required PLA chain length is not

possible with FNP. The slow diffusion coefficient of a significantly larger PEG_m-PLA_n polymer would change the dynamics of the assembly process, which requires matching the hydrophobic drug aggregation kinetics to polymer diffusion and adsorption kinetics [21].

(3) *The absolute molecular weight of the PEG block*. Fig. 4 shows that the percent of nanocarriers in circulation after 4 h for the PEG_{5k}-PCL_{7k}, PEG_{5k}-PCL_{3k}, and PEG_{2k}-PCL_{3k} were 40%, 58%, and 18%, respectively. With the same 3k PCL anchoring block the 5k PEG block is three times more effective than the 2k PEG block. This behavior where 5k PEG chains are more protective than 2k chains has been observed previously [41]. The mechanism of protection is associated with both the thickness of the layer and the entropic penalty of deforming a chain. There is a greater entropic penalty to deform the larger PEG chain, and therefore, the absolute size of the PEG plays a role [42]. It might be argued that Rule 1 is the cause of greater effectiveness, specifically stemming from a greater PEG packing density due to the larger PEG size relative to the PCL size. However, the PEG_{5k}-PCL_{7k} and the PEG_{2k}-PCL_{3k} are almost equally balanced in the relative sizes of blocks, yet the 5k PEG block copolymer is twice as effective as the 2k PEG polymer, which confirms that the absolute PEG size in the block copolymer makes a difference in nanocarrier protection. At this point, we have not studied higher Mw PEG blocks to assess their effectiveness.

(4) The amorphous/crystalline nature of the hydrophobic block. The poorest circulating nanocarriers were formed with the PEG_{5k}-PCL_{9k}. While the poor circulation of this construct could be ascribed to Rule 1 (relative block sizes), there is another factor that dominates the surface coverage. Crystallization studies of PEG-PCL diblock and triblock copolymers have revealed an increase in the PCL block crystallinity with increasing PCL Mw. A study by He *et al.* using wide angle X-ray diffraction (WAXD) observed lower crystallizability of PEG-PCL with $Mw_{PEG}/Mw_{PCL} > 1$, compared with diblocks of larger PCL blocks in the range 2,000 to 30,000 g/mole [43]. In our experiments, PEG_{5k}-PCL_{5k} corresponds to $Mw_{PEG}/Mw_{PCL} = 1$, while PEG_{5k}-PCL_{9k} corresponds to $Mw_{PEG}/Mw_{PCL} = 0.556$. It is expected that the 9k PLC block should recrystallize after assembly. This crystallization disrupts the PEG surface coverage. We have previously observed this result for nanocrystals coated in FNP by PEG_{5k}-PCL_{7k}, where $Mw_{PEG}/Mw_{PCL} = 0.714$ [31].

Fig. 4 shows 85% of the PEG_{3k}-PS_{1k} stabilized nanocarriers remained in circulation 4 h following administration, which indicates substantially better stabilization *in vivo* than the other block copolymers. As previously noted, nanocarriers stabilized by this polymer can achieve circulation half-times as long as 24 h [2]. The enhanced stability results from two main factors. First, the PS block is the most hydrophobic of the block chemistries explored in this work; thus, there is sufficient energy to anchor the block copolymer even though the Mw is relatively low (Rule 2). Second, the PEG block is twice as large as the anchoring block. This creates crowding and dense PEG packing on the nanocarrier surface (Rule 1). The larger PEG size relative to the anchoring block is effective for the PS chain with its high hydrophobicity. It is less effective for the PEG_{5k}-PCL_{3k} because the lower hydrophobicity of the PCL block does not enable the formation of a layer of densely packed and crowded chains.

3.2. Complement activation assay

In the complement activation experiments, the hydrophilic PEG block size was held constant at 5k in order to isolate the effects of the hydrophobic block on the nanocarrier protection. Images of the stained gel slabs for each nanocarrier sample after incubation with complement proteins are collected in Fig. 3a. The peak on the left represents the non-activated complement protein that has not interacted with the hydrophobic nanocarrier surface, and the peak on the right represents activated complement fragments. The ratio of

the area under the two peaks visually indicates the level of protection, and is quantified according to Eq. 4 to yield the Complement Activation Factor, CAF. Nearly all images appear qualitatively similar, with the left peak being significantly higher than the right peak, indicating low activation of complement. Only the nanocarrier stabilized by PEG_{5k}-PCL_{9k}, shows a marked difference, with a significantly larger peak to the right. The *CAF* for each nanocarrier formulation is plotted in Fig. 3b, with CAF values in the range from 1 ± 1 to 12 ± 4 for well protected formulations. As was qualitatively observed, PEG_{5k}-PCL_{9k} activates complement strongly, with a $CAF_{PEG5k\text{-}PCL9k} = 86 \pm 2$. There were no samples that demonstrated moderate complement activation.

We find that the all of the formulations with amorphous hydrophobic blocks, which include PS, PLA, and PLGA, enable sufficient stabilization of the nanocarriers so that there is little complement activation over the incubation period in the assay. There was no detectable dependence on the size of the hydrophobic block for PS, PLA, or PLGA. In contrast to block copolymers with amorphous hydrophobic blocks, we find that that there is a threshold value of the PCL M*w* for formulations stabilized by PEG-PCL block copolymers, above which, the particle formulation is a strong complement activator. While the PEG_{5k}-PCL_{5k} stabilized particles show low complement activation, the particles stabilized with PEG_{5k}-PCL_{9k} are found to be strong complement activators. Therefore, a subtle change in M*w* dramatically changes the protection of the nanocarriers from interaction with the complement protein. From these results, it becomes clear that investigating complement activation *in vitro* can only determine those formulations which would be rapidly cleared from circulation. An alternative *in vitro* characterization technique is needed to capture the more subtle differences observed in the *in vivo* as a function of block copolymer architecture.

3.3. PEG surface conformation

To provide evidence for Rule 1, we quantify the effect of the hydrophobic block M*w* on the packing density of PEG at the interface. According to the protocol developed by Budijono, *et al.,* surfactant-free, 200 nm latex spheres were coated by FNP with block copolymers and the Baleux Assay was used to quantify the concentration of PEG coated on the latex spheres [27]. The separation protocol was adapted to permit measurement of the PEG concentration in both the pellet and supernatant, without significant error due to light scattering. The relationship between sample absorbance and the concentration of PEG-PCL, PEG-PLA, and PEG-PS micelles was determined using polymer concentrations between 1 and 20 mg/L in 3.3% THF-water as dictated by the Baleux assay protocol.

The calculated PEG blob size, ξ_{exp}, for each block copolymer is plotted as a function of the hydrophobic block M*w* in Fig. 6 and increases monotonically with increasing block size, indicating that the PEG chains become less crowded as the M*w* increases. This supports the hypothesis that the hydrophobic chain M*w* influences the PEG chain packing and protection on the surface of the particle, according to Rule 1. To determine the PEG chain conformation for these formulations, $\xi_{mushroom}$ and ξ_{brush} were calculated for reference as described previously [27]. The Flory size (which is also the mushroom size for the unconstrained chain at the interface) depends on the PEG M*w*, and was calculated as $\xi_{mushroom} = 5.3$ nm for all of the 5k PEG. The experimental PEG blob size is well below the mushroom blob size when the hydrophobic block has a low M*w*. However, as the hydrophobic block M*w* increases, as is the case for PLA_{20k}, the PEG conformation is closer to the mushroom regime (Fig. 6b). Using available data for the interfacial energy of PEG [27], PCL [44–47], PS [48, 49], and PLA [50], we calculate the theoretical values for ξ_{brush} for a PEG_{5k} chain following the development used by Budijono, *et al* [27]. Since multiple experimental values for the interfacial energy are reported, several values for ξ_{brush} are calculated and are plotted to indicate the range of the brush regime. These values are plotted

in Fig. 6 where they show that the experimental PEG packing density achieved by FNP is in the brush regime when the hydrophobe M*w* is low.

As the PCL chain sizes increase, and the packing density of the PEG decreases (Fig. 6a), we observe that the formulations have increased clearance rates from circulation (Fig. 4). Since the effectiveness of steric stabilization of nanocarrier surfaces from protein binding depends on a high entropic penalty for displacing or compressing PEG chains, it follows that less crowded chains are less effective. This *in vitro* assay demonstrates a correlation between the density of the PEG surface packing and *in vivo* differences in the elimination of nanocarriers, formed by FNP, from circulation in mice. While data has been previously presented correlating PEG density on liposomes with *in vivo* clearance, we believe this is the first demonstration with solid hydrophobic nanocarriers that *in vivo* clearance is correlated with a quantitative *in vitro* measurement of PEG surface density.

4. Summary and Conclusions

Achieving specificity in drug delivery is important to avoid unwanted side effects associated with systemic delivery of therapeutic agents and to maximize therapeutic efficacy. Targeting requires long circulation times and, hence, protection from recognition and clearance by nonspecific mechanisms of the immune system. In this study of nanocarriers formed by kinetically controlled, block copolymer-directed assembly *via* Flash NanoPrecipitation, we find substantial differences in *in vivo* circulation times depending on the block copolymer structure. The results lead us to propose four guidelines for the engineering of stabilizing polymers for these PEG-protected nanocarriers: 1) The relative anchoring area of the hydrophobic block to that of the solvated PEG chain, 2) The hydrophobicity or anchoring strength of the hydrophobic block relative to the solvation energy of the hydrophilic block, 3) The absolute M*w* of the PEG block, and 4) The amorphous/crystalline nature of the hydrophobic block. For the polymers we have considered, the hydrophobic blocks are of sufficient M*w* that partitioning off of the nanocarrier surface does not determine the circulation effectiveness. However, for less hydrophobic blocks or blocks of even smaller M*w*, partitioning off of the surface may be a significant factor in determining circulation. While this work has focused on improving the circulation of nanocarriers by determining the effects of the block copolymer structure, this formulation component may also affect delivery by changing drug release rates, and further study into these effects is warranted.

An *in vitro* complement activation assay was employed to test for a correlation between the *in vivo* and *in vitro* results. The complement assay could readily detect the difference between the very poorly circulating PEG_{5k}-PCL_{9k} stabilized nanocarriers and the other formulations. However, it could not differentiate the gradations in circulation times for the other block copolymers. Whether this is due to clearance in mice arising from other pathways not associated with complement activation, or due to lack of sensitivity in the complement assay is not known. Quantifying the PEG blob size as a function of PCL M*w* on hydrophobic latex spheres reveals that the density of the PEG layer decreases as the PCL block increases in size and the *in vivo* clearance does correlate with this measure of PEG density. Further work to enhance the sensitivity of the complement assay is warranted. Other complement assays [17] or immune system compatibility assays [51] could be attempted to determine if they exhibit different sensitivities than the version of the assay we have employed for this study. Proteomics-based assays might show more subtle differences in cellular response to nanocarrier interactions and might be another possible avenue to pursue.

Supplementary Material

Refer to Web version on PubMed Central for supplementary material.

Acknowledgments

The authors thank Brit Nacke (Univ Paris Sud) for her assistance in performing complement activation evaluation. This research was supported with funding from the National Science Foundation NIRT award (CBET-0506966) and the NIH (RO1 CA155061-01). ADW, TRH, and CWM thank the National Institutes of Health (NIBIB EB011671) and the University of Minnesota Futures program for financial support.

Role of the funding sources

The sponsors played no role in the design, collection, or interpretation of the data, or writing of the manuscript.

References

1. Alexis F, Pridgen E, Molnar LK, Farokhzad OC. Factors affecting the clearance and biodistribution of polymeric nanoparticles. Mol Pharm. 2008; 5(4):505–515. [PubMed: 18672949]
2. Ansell SM, Johnstone SA, Tardi PG, Lo L, Xie SW, Shu Y, Harasym TO, Harasym NL, Williams L, Bermudes D, Liboiron BD, Saad W, Prud'homme RK, Mayer LD. Modulating the therapeutic activity of nanoparticle delivered paclitaxel by manipulating the hydrophobicity of prodrug conjugates. J Med Chem. 2008; 51(11):3288–3296. [PubMed: 18465845]
3. Acharya S, Sahoo SK. PLGA nanoparticles containing various anticancer agents and tumour delivery by EPR effect. Adv Drug Deliver Rev. 2011; 63(3):170–183.
4. Matsumura Y, Maeda H. A New Concept for Macromolecular Therapeutics in Cancer-Chemotherapy - Mechanism of Tumoritropic Accumulation of Proteins and the Antitumor Agent Smancs. Cancer Res. 1986; 46(12):6387–6392. [PubMed: 2946403]
5. Stolnik S, Dunn SE, Garnett MC, Davies MC, Coombes AGA, Taylor DC, Irving MP, Purkiss SC, Tadros TF, Davis SS, Illum L. Surface Modification of Poly(Lactide-Co-Glycolide) Nanospheres by Biodegradable Poly(Lactide)-Poly(Ethylene Glycol) Copolymers. Pharm Res. 1994; 11(12):1800–1808. [PubMed: 7899246]
6. Jokerst JV, Lobovkina T, Zare RN, Gambhir SS. Nanoparticle PEGylation for imaging and therapy. Nanomedicine-UK. 2011; 6(4):715–728.
7. Owens DE, Peppas NA. Opsonization, biodistribution, and pharmacokinetics of polymeric nanoparticles. Int J Pharm. 2006; 307(1):93–102. [PubMed: 16303268]
8. Kenworthy AK, Simon SA, Mcintosh TJ. Structure and Phase-Behavior of Lipid Suspensions Containing Phospholipids with Covalently Attached Poly(Ethylene Glycol). Biophys J. 1995; 68(5): 1903–1920. [PubMed: 7612833]
9. Ashbaugh HS, Boon K, Prud'homme RK. Gelation of "catanionic" vesicles by hydrophobically modified polyelectrolytes. Colloid Polym Sci. 2002; 280(9):783–788.
10. Auguste DT, Prud'homme RK, Ahl PL, Meers P, Kohn J. Association of hydrophobically-modified poly(ethylene glycol) with fusogenic liposomes. BBA-Biomembranes. 2003; 1616(2): 184–195. [PubMed: 14561476]
11. Ligoure C, Leibler L. Thermodynamics and Kinetics of Grafting End-Functionalized Polymers to an Interface. J Phys-Paris. 1990; 51(12):1313–1328.
12. Degennes PG. Conformations of Polymers Attached to an Interface. Macromolecules. 1980; 13(5): 1069–1075.
13. Feng W, Brash JL, Zhu SP. Non-biofouling materials prepared by atom transfer radical polymerization grafting of 2-methacryloloxyethyl phosphorylcholine: Separate effects of graft density and chain length on protein repulsion. Biomaterials. 2006; 27(6):847–855. [PubMed: 16099496]
14. Himmelhaus M, Bastuck T, Tokumitsu S, Grunze M, Livadaru L, Kreuzer HJ. Growth of a dense polymer brush layer from solution. Europhys Lett. 2003; 64(3):378–384.
15. Bertholon I, Vauthier C, Labarre D. Complement activation by core-shell poly(isobutylcyanoacrylate)-polysaccharide nanoparticles: Influences of surface morphology, length, and type of polysaccharide. Pharm Res. 2006; 23(6):1313–1323. [PubMed: 16715369]

16. Boackle RJ, Caughman GB, Vesely J, Medgyesi G, Fudenberg HH. Potentiation of Factor-H by Heparin - a Rate-Limiting Mechanism for Inhibition of the Alternative Complement Pathway. Mol Immunol. 1983; 20(11):1157–1164. [PubMed: 6228720]

17. Cooper NR, Nemerow GR, Mayes JT. Methods to Detect and Quantitate Complement Activation. Springer Semin Immun. 1983; 6(2–3):195–212.

18. Henry SP, Giclas PC, Leeds J, Pangburn M, Auletta C, Levin AA, Kornbrust DJ. Activation of the alternative pathway of complement by a phosphorothioate oligonucleotide: Potential mechanism of action. J Pharmacol Exper Ther. 1997; 281(2):810–816. [PubMed: 9152389]

19. Mosqueira VCF, Legrand P, Gulik A, Bourdon O, Gref R, Labarre D, Barratt G. Relationship between complement activation, cellular uptake and surface physicochemical aspects of novel PEG-modified nanocapsules. Biomaterials. 2001; 22(22):2967–2979. [PubMed: 11575471]

20. Passirani C, Barratt G, Devissaguet JP, Labarre D. Interactions of nanoparticles bearing heparin or dextran covalently bound to poly(methyl methacrylate) with the complement system. Life Sci. 1998; 62(8):775–785. [PubMed: 9489513]

21. Johnson BK, Prud'homme RK. Chemical processing and micromixing in confined impinging jets. AICHE J. 2003; 49(9):2264–2282.

22. Liu Y, Cheng CY, Liu Y, Prud'homme RK, Fox RO. Mixing in a multi-inlet vortex mixer (MIVM) for flash nano-precipitation. Chem Eng Sci. 2008; 63(11):2829–2842.

23. Chen T, D'Addio SM, Kennedy MT, Swietlow A, Kevrekidis IG, Panagiotopoulos AZ, Prud'homme RK. Protected Peptide Nanoparticles: Experiments and Brownian Dynamics Simulations of the Energetics of Assembly. Nano Lett. 2009; 9(6):2218–2222. [PubMed: 19413305]

24. Chiou H, Chan HK, Heng D, Prud'homme RK, Raper JA. A novel production method for inhalable cyclosporine A powders by confined liquid impinging jet precipitation. J Aerosol Sci. 2008; 39(6): 500–509.

25. Kumar V, Hong SY, Maciag AE, Saavedra JE, Adamson DH, Prud'homme RK, Keefer LK, Chakrapani H. Stabilization of the Nitric Oxide (NO) Prodrugs and Anticancer Leads, PABA/NO and Double JS-K, through Incorporation into PEG-Protected Nanoparticles. Mol Pharm. 2010; 7(1):291–298. [PubMed: 20000791]

26. Kumar V, Wang L, Riebe M, Tung HH, Prud'homme RK. Formulation and Stability of ltraconazole and Odanacatib Nanoparticles: Governing Physical Parameters. Mol Pharm. 2009; 6(4):1118–1124. [PubMed: 19366261]

27. Budijono SJ, Russ B, Saad W, Adamson DH, Prud'homme RK. Block copolymer surface coverage on nanoparticles. ColloidSurface A. 2010; 360(1–3):105–110.

28. Zhang SY, Adamson DH, Prud'homme RK, Link AJ. Photocrosslinking the polystyrene core of block-copolymer nanoparticles. Polym Chem. 2011; 2(3):665–671.

29. Lohmeijer BGG, Pratt RC, Leibfarth F, Logan JW, Long DA, Dove AP, Nederberg F, Choi J, Wade C, Waymouth RM, Hedrick JL. Guanidine and amidine organocatalysts for ring-opening polymerization of cyclic esters. Macromolecules. 2006; 39(25):8574–8583.

30. Qian HT, Wohl AR, Crow JT, Macosko CW, Hoye TR. A Strategy for Control of "Random" Copolymerization of Lactide and Glycolide: Application to Synthesis of PEG-b-PLGA Block Polymers Having Narrow Dispersity. Macromolecules. 2011; 44(18):7132–7140. [PubMed: 22287809]

31. Budijono SJ, Shan JN, Yao N, Miura Y, Hoye T, Austin RH, Ju YG, Prud'homme RK. Synthesis of Stable Block-Copolymer-Protected NaYF(4):Yb(3+), Er(3+) Up-Converting Phosphor Nanoparticles. Chem Mater. 2010; 22(2):311–318.

32. Shuai XT, Merdan T, Unger F, Wittmar M, Kissel T. Novel biodegradable ternary copolymers hy-PEI-g-PCL-b-PEG: Synthesis, characterization, and potential as efficient nonviral gene delivery vectors. Macromolecules. 2003; 36(15):5751–5759.

33. Rasband, WS. ImageJ. U. S. National Institutes of Health; Bethesda, Maryland, USA: 1997–2011. http://imagej.nih.gov/ij/

34. Molinspiration Cheminformatics, Nova ulica, SK-900 26 Slovensky Grob, Slovak Republic. www.Molinspiration.com

35. Baleux B. Colorimetric Determination of Silver of Nonionic Polyoxyethylene Surface Using Iodo-Iodated Solution. CR Acad Sci C Chim. 1972; 274(19):1617.
36. Pool GL, French ME, Edwards RA, Huang L, Lumb RH. Use of Radiolabeled Hexadecyl Cholesteryl Ether as a Liposome Marker. Lipids. 1982; 17(6):448–452. [PubMed: 7050582]
37. Kumar V, Adamson DH, Prud'homme RK. Fluorescent Polymeric Nanoparticles: Aggregation and Phase Behavior of Pyrene and Amphotericin B Molecules in Nanoparticle Cores. Small. 2011; 6(24):2907–2914. [PubMed: 21104798]
38. Vauthier C, Persson B, Lindner P, Cabane B. Protein adsorption and complement activation for di-block copolymer nanoparticles. Biomaterials. 2011; 32(6):1646–1656. [PubMed: 21093043]
39. Reed AM, Gilding DK. Biodegradable Polymers for Use in Surgery - Poly(Glycolic)-Poly(Lactic Acid) Homo and Co-Polymers .2. Invitro Degradation. Polymer. 1981; 22(4):494–498.
40. Kozlov MY, Melik-Nubarov NS, Batrakova EV, Kabanov AV. Relationship between pluronic block copolymer structure, critical micellization concentration and partitioning coefficients of low molecular mass solutes. Macromolecules. 2000; 33(9):3305–3313.
41. Gref R, Luck M, Quellec P, Marchand M, Dellacherie E, Harnisch S, Blunk T, Muller RH. 'Stealth' corona-core nanoparticles surface modified by polyethylene glycol (PEG): influences of the corona (PEG chain length and surface density) and of the core composition on phagocytic uptake and plasma protein adsorption. Colloid Surface B. 2000; 18(3–4):301–313.
42. Harder P, Grunze M, Dahint R, Whitesides GM, Laibinis PE. Molecular conformation in oligo(ethylene glycol)-terminated self-assembled monolayers on gold and silver surfaces determines their ability to resist protein adsorption. J Phys Chem B. 1998; 102(2):426–436.
43. He CL, Sun J, Deng C, Zhao T, Deng MX, Chen XS, Jing XB. Study of the synthesis, crystallization, and morphology of poly(ethylene glycol)-poly(epsilon-caprolactone) diblock copolymers. Biomacromolecules. 2004; 5(5):2042–2047. [PubMed: 15360322]
44. Biresaw G, Carriere CJ. Correlation between mechanical adhesion and interfacial properties of starch/biodegradable polyester blends. J Polym Sci Pol Phys. 2001; 39(9):920–930.
45. Normand F, Granier A, Leprince P, Marec J, Shi MK, Clouet F. Polymer Treatment in the Flowing Afterglow of an Oxygen Microwave-Discharge - Active Species Profile Concentrations and Kinetics of the Functionalization. Plasma Chem Plasma P. 1995; 15(2):173–198.
46. Erbil HY, Yasar B, Suzer S, Baysal BM. Surface characterization of the hydroxy-terminated poly(epsilon-caprolactone)/poly(dimethylsiloxane) triblock copolymers by electron spectroscopy for chemical analysis and contact angle measurements. Langmuir. 1997; 13(20):5484–5493.
47. Yasin M, Tighe BJ. Polymers for Biodegradable Medical Devices .8. Hydroxybutyrate Hydroxyvalerate Copolymers - Physical and Degradative Properties of Blends with Polycaprolactone. Biomaterials. 1992; 13(1):9–16. [PubMed: 1543811]
48. Wu S. Surface and Interfacial Tensions of Polymer Melts .2. Poly(Methyl Methacrylate), Poly(Normal-Butyl Methacrylate), and Polystyrene. J Phys Chem. 1970; 74(3):632.
49. Wu S. Surface and Interfacial Tensions of Polymer Melts .I. Polyethylene, Polyisobutylene, and Polyvinyl Acetate. J Colloid Interf Sci. 1969; 31(2):153.
50. Biresaw G, Carriere CJ. Interfacial tension of poly(lactic acid)/polystyrene blends. J Polym Sci Pol Phys. 2002; 40(19):2248–2258.
51. Dobrovolskaia MA, Aggarwal P, Hall JB, McNeil SE. Preclinical studies to understand nanoparticle interaction with the immune system and its potential effects on nanoparticle biodistribution. Mol Pharm. 2008; 5(4):487–495. [PubMed: 18510338]

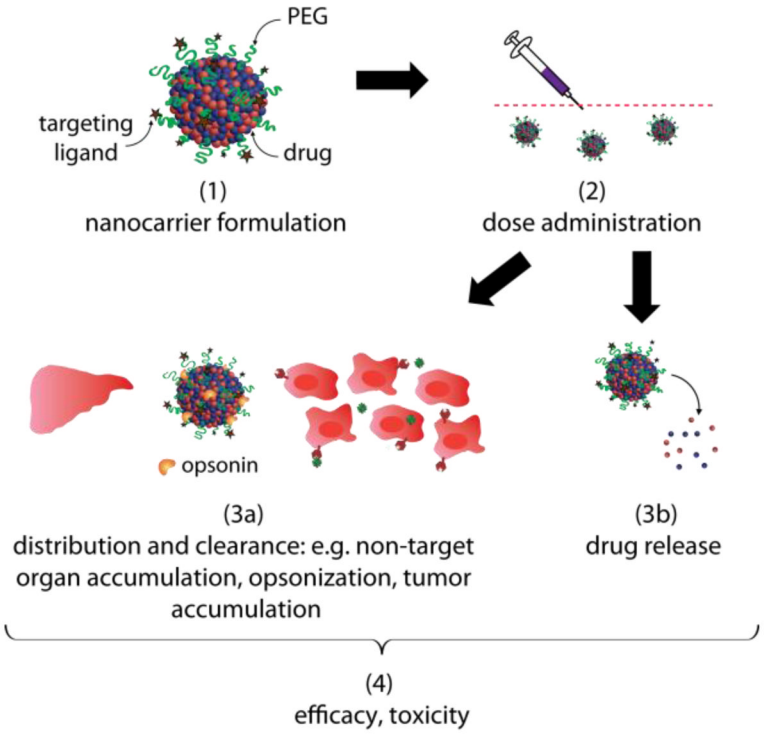

Figure 1.
General scheme for drug therapy by nanocarrier delivery. (1) Nanocarriers may be formulated with a drug core, PEG stabilizing corona, and targeting ligands. In this work, a hydrophobic paclitaxel prodrug is used and stabilized by a PEG corona. (2) Nanocarriers in suspension are administered intravenously. (3a) Nanocarriers in circulation may accumulate at the tumor site passively, by specific binding, or be eliminated by distribution to tissues or through immune recognition. (3b) The drug payload is be released from the nanocarrier core. The relative timescales for these events (3a and b) is formulation dependent and contribute to (4) the efficacy or toxicity of the formulation.

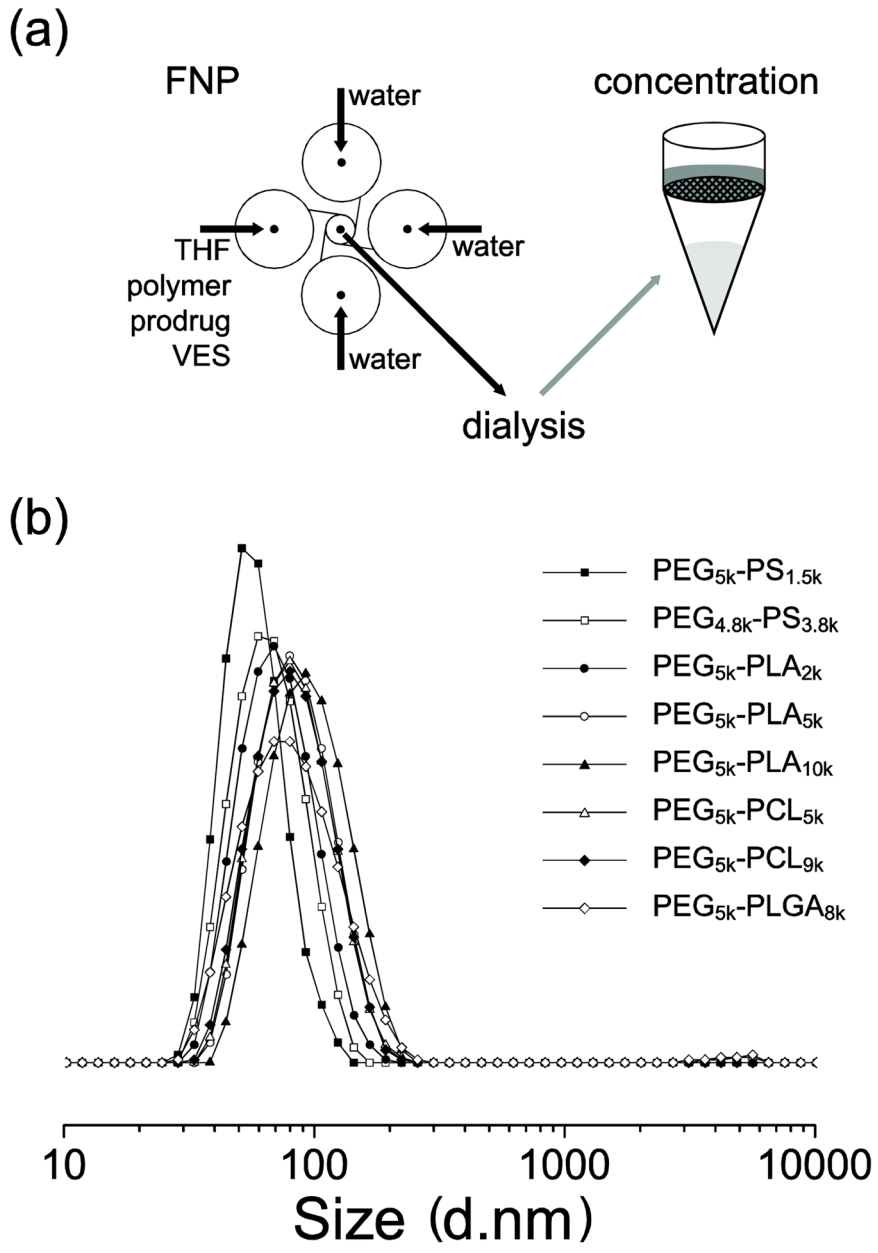

Figure 2.

(a) General scheme for nanocarrier formulation by FNP. After mixing solvent streams in a multi inlet vortex mixer (MIVM), the suspension is dialyzed against water to remove the organic solvent. Specifically, prior to complement activation experiments, the suspensions are concentrated by removal of water through a membrane by centrifugation. (b) The intensity weighted particle size distributions for each of the vitamin E nanocarrier formulations tested in the complement activation experiments as determined by dynamic light scattering. The narrow size distributions justify the use of the peak mean value of the diameter in the approximation of nanocarrier surface area concentration.

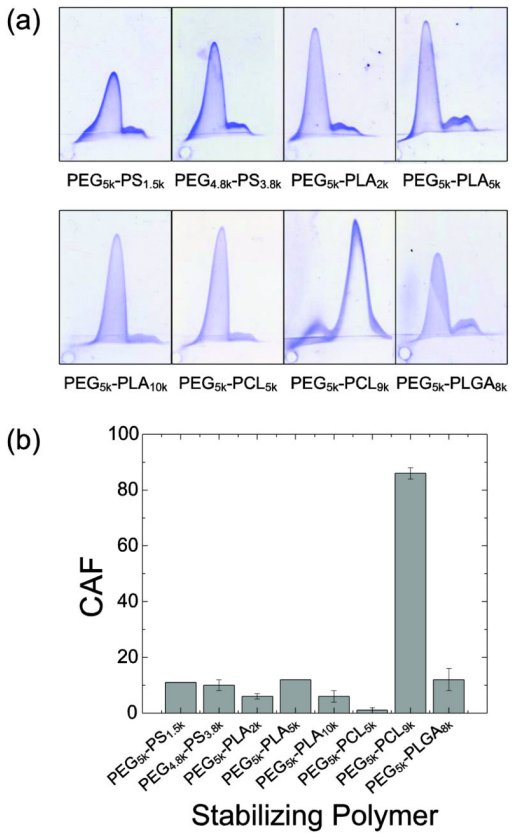

Figure 3.

Complement activation results. (a) The digitized gel slabs, obtained through 2D electrophoresis of nanocarriers incubated with complement proteins, were scanned three time and analyzed to obtain the area of each peak associated with the native C3 protein (left) and the activated C3ab fragments (right). (b) The Complement Activation Factor (CAF) quantifies the extent to which each formulation activated the complement protein. For each CAF, the average value and the standard deviation corresponds to the average of three separate experiments, in which each gel slab was scanned and analyzed three times.

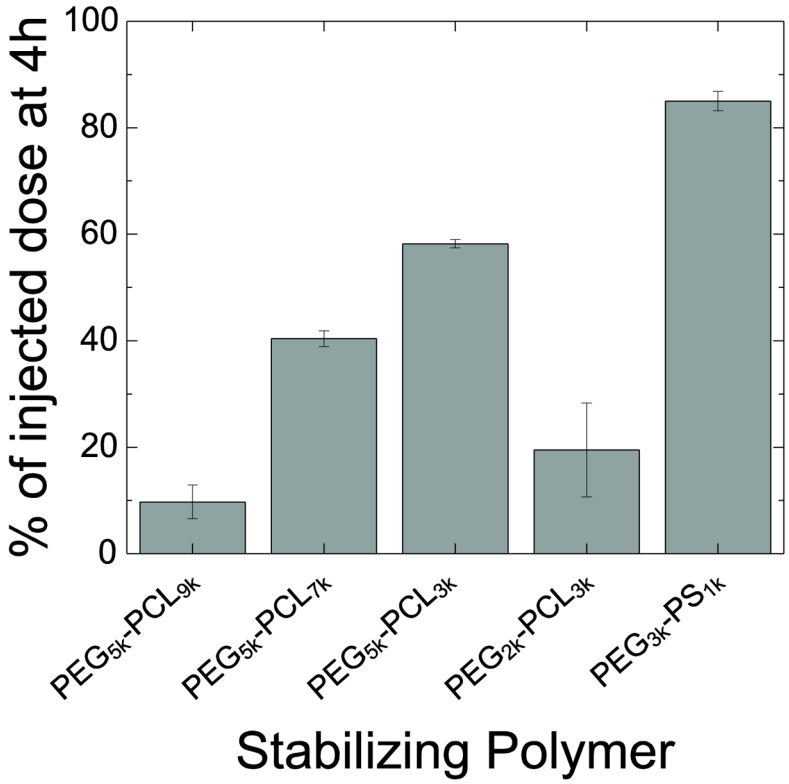

Figure 4.

The amount of prodrug remaining in circulation *in vivo* 4 h after IV injection (n = 3/time point), as quantified via HPLC of a plasma sample, for prodrug nanocarriers stabilized by the 5 indicated block copolymers. Error bars represent standard deviation of the mean.

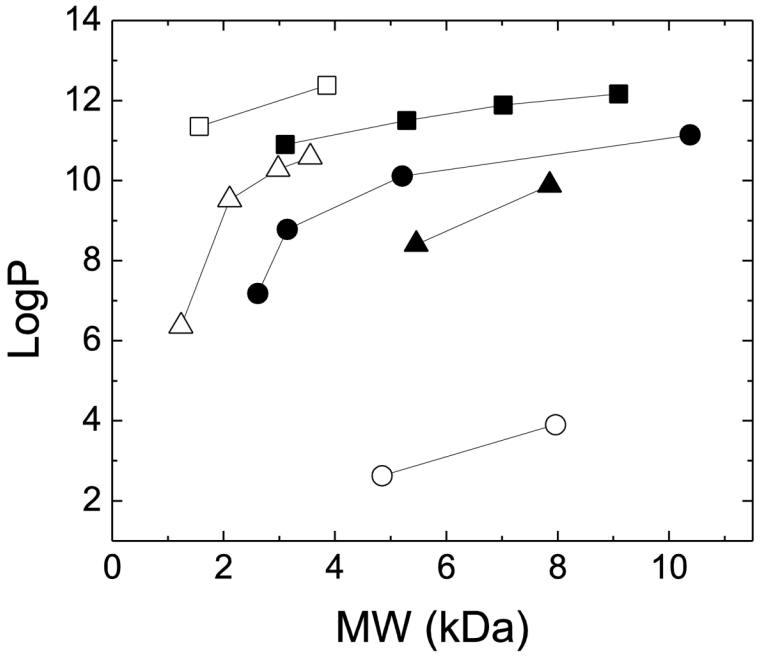

Figure 5.
The calculated log*P* values for homopolymer PCL (■), PS (□), PLA (●), PLGA 50/50 (○), PLGA 75/25 (▲), and PPO (△), plotted as a function of hydrophobic homopolymer M*w*, which is an indication of the hydrophobicity and ability to anchor PEG to the nanocarrier surface.

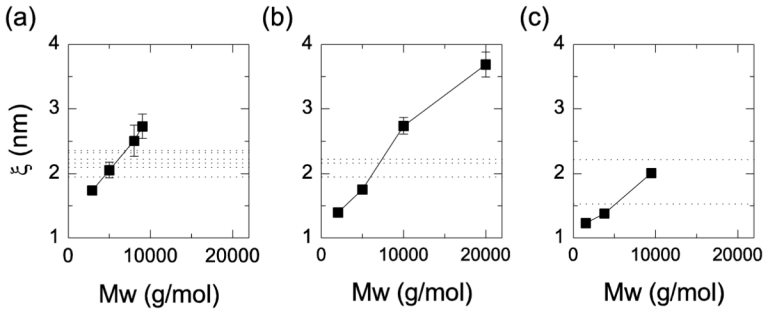

Figure 6.

Experimentally determined blob diameter, ξ_{exp}, of PEG coated on the surface of 200 nm surfactant-free latex spheres. Data is presented as ξ_{exp} for PEG_{5k} with hydrophobic blocks of (a) PCL (b) PLA and (c) PS with various M*w*. The values for $\xi_{brush,}$ in the brush regime, are calculated according to Budijono, *et al.* [27], and are indicated by dashed lines. Several literature values for the surface tension of PCL [44–47], PS [48, 49], and PLA [50] were used to calculate the different theoretical values for ξ_{brush}. The mushroom blob size is $\xi_{mushroom}$ = 5.3 nm. The error bars correspond to the standard deviation for the ξ_{exp} measured on 3 replicate samples.

Table 1

Nanocarriers for *in vivo* circulation studies.

Formulation	Stabilizing Polymer	Aqueous suspension composition after FNP (mg/mL)			Average diameter ± SD[a] (nm)
		Polymer	VES	Prodrug	
1	PEG_{5k}-PCL_{9k}	0.92	0.46	0.46	80 ± 19
2	PEG_{5k}-PCL_{7k}	1.16	0.58	0.58	84 ± 18
3	PEG_{5k}-PCL_{3k}	1.34	0.67	0.67	104 ± 28
4	PEG_{2k}-PCL_{3k}	1.02	0.51	0.51	66 ± 15
5	PEG_{3k}-PS_{1k}	0.8	0.4	0.4	72 ± 16

[a]The standard deviation (SD) represents the width of one standard deviation for the log normal particle size distribution.

Table 2

Nanocarriers for complement activation studies.

Formulation	Stabilizing Block Copolymer	$c_{BCP,THF}$[a] (mg/mL)	$c_{VE,THF}$[b] (mg/mL)	$c_{NR,THF}$[c] (μg/mL)	d[d] (nm)	c_P[e] (mg/mL)	S_pN[f] (cm²/mL)
6	PEG_{5k}-$PS_{1.5k}$	10	5	25	58 ± 7	12	1.3×10^4
7	$PEG_{4.8k}$-$PS_{3.8k}$	10	10	50	67 ± 1	12	1.0×10^4
8	PEG_{5k}-PLA_{2k}	10	5	25	73 ± 5	16	1.3×10^4
9	PEG_{5k}-PLA_{5k}	10	10	50	86 ± 1	11	7.8×10^3
10	PEG_{5k}-PLA_{10k}	10	10	50	98 ± 2	17	1.1×10^4
11	PEG_{5k}-PCL_{5k}	10	10	50	85 ± 6	16	1.1×10^4
12	PEG_{5k}-PCL_{9k}	10	2.5	12.5	85 ± 2	19	1.4×10^4
13	PEG_{5k}-$PLGA_{8k}$	10	5	25	84 ± 1	13	9.2×10^3

[a] $c_{BCP,THF}$, concentration of block copolymer in THF;

[b] $c_{VE,THF}$, concentration of vitamin E in THF;

[c] $c_{NR,THF}$, concentration of nile red in THF;

[d] d, intensity weighted average diameter, reported ± the standard deviation of three measurements;

[e] c_P, concentration of nanocarriers after concentration;

[f] S_pN: nanocarrier surface area per mL of solution, calculated according to Eq. 2.